ChemComm

Accepted Manuscript

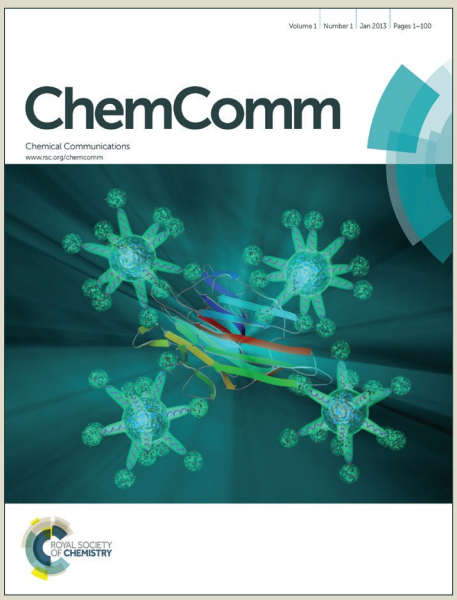

ROYAL SOCIETY OF CHEMISTRY

www.rsc.org/chemcomm

Journal Name

COMMUNICATION

A photoelectrochemical methanol fuel cell based on aligned TiO_2 nanorods decorated graphene photoanode

Received 00th January 20xx,
Accepted 00th January 20xx

DOI: 10.1039/x0xx00000x

www.rsc.org/

Xinyuan Li, [a] Guowen Wang, [b] Lin Jing, [a] Wei Ni, [a] Huan Yan, [a] Chao Chen, [a] Yi-Ming Yan* [a]

We report the photoelectrochemical (PEC) oxidation of methanol on a rational designed graphene-TiO_2 nanorod arrays (G-TNRs) photoanode. A PEC methanol fuel cell is constructed by coupling G-TNRs photoanode with a cathode. This work raises a conceptual fuel cell that realizing synergistic energy conversion of chemical energy and solar energy.

Photoelectrochemical (PEC) fuel cell [1-7] using sunlight as energy input is a promising strategy to deal with both environmental pollution and energy crisis. PEC fuel cell is mainly composed of a semiconductor photoanode, a cathode, and the electrolyte that containing organic fuels (such as glucose, alcohol, methanol, formic acid). Upon light illumination, semiconductor on the anode can generate a large amount of electron-hole pairs. The holes can efficiently oxidize organic fuels at the photoanode, while the electrons can be transferred to cathode, where the oxygen reduction reaction (ORR) is occurred. Taking this advantage, PEC fuel cell can convert chemical energy into electricity in much efficient way with the assistance of sunlight.

The photocatalyt plays crucial role as it determines the energy conversion efficiency of a PEC fuel cell. In order to photocatalytically oxidize the fuels, efforts have been devoted to find efficient photocatalysts for photoanode. Metal oxide semiconductors, such as WO_3 [8], SnO_2 [9], ZnO [10-12], $BiVO_4$ [13], TiO_2 [11, 12, 14, 15], have been intensively investigated due to their appropriate band gap, low electrical resistance, low cost, and easy production [12]. Among these photocatalysts, TiO_2 shows unique advantages of excellent photocatalytic activity, high chemical and photochemical stability [11, 12, 14-17]. Unfortunately, the use of TiO_2 has been largely limited by its low absorbance of visible light, rapid charge recombination and low charge transfer efficiency during the PEC process. To solve above problems, several strategies, such as coupling TiO_2 with other semiconductors [11, 12], deposition of noble metal as co-catalysts [15, 18], doping elements [19, 20], and dye sensitization [21], have been reported.

It is known that the morphology and structure of TiO_2 could affect its photocatalytic performance. Particularly, TiO_2 nanorod, with one-dimension (1D) structure, has shown unique advantages in photocatalytical applications because that 1D structure could offer direct pathways for photo-generated electrons transfer, which can enhance the efficiency of charge separation. [12, 22-24] Furthermore, 1D structured catalysts possess larger active surface-to-volume ratio, [22, 24] which can facilitate the photocatalytic reaction in the electrolyte. On the other hand, graphene has been regarded as a competitive host substance for the growth of TiO_2 due to its large surface area, superior electrical conductivity, high optical transmittance and excellent mechanical stability. [25-27] However, to the best of our knowledge, no study has been reported yet in the literature related to the preparation of TiO_2 nanorods modified graphene and its photocatalyical performance, especially for its application as a photoanode of PEC fuel cell.

In this work, we demonstrate the design and synthesis of the TiO_2 nanorods modified graphene (G-TNRs) as novel structured photocatalyst. The G-TNRs modified electrode was used as a photoanode of PEC fuel cell. The prepared G-TNRs showed significantly enhanced activities towards photoelectrochemical (PEC) oxidation of methanol. To construct a methanol fuel cell, the 3D interpenetrating nanostructured graphene nanosheets-carbon nanotubes (GN-CNT) hybrid was prepared according to our previous work and used as cathode for oxygen reduction. [28] With this novel PEC fuel cell configuration, electricity was successfully extracted by using methanol fuel. We noted that, although direct methanol fuel cell based on noble metal catalysts has been investigated, here we demonstrate a novel concept of PEC methanol fuel cell based on photoanode by using the sunlight as a synergistic energy input. We believe that this work not only offers insights into the design of functional materials with controllable properties for

[a] School of Chemical Engineering and Environment, Beijing Institute of Technology, Beijing, 100081, People's Republic of China
[b] Beijing Aerospace Propulsion Institute, Beijing, 10076, People's Republic of China.
Email: bityanyiming@163.com;
Electronic Supplementary Information (ESI) available: [Experimental details, SEM, SAED, XRD, XPS, FTIR, photocurrent-wavelength curves and stability test can be found in the ESI]. See DOI: 10.1039/x0xx00000x

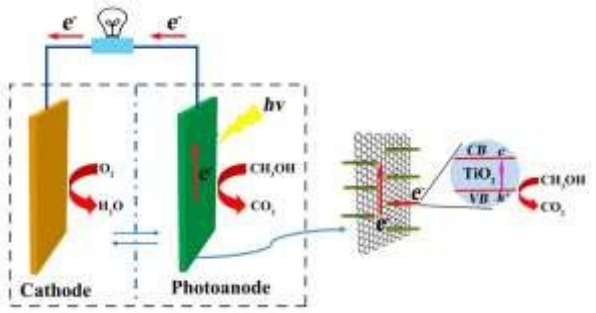

Fig.1 Schematic diagram of photoelectrochemical methanol fuel cell.

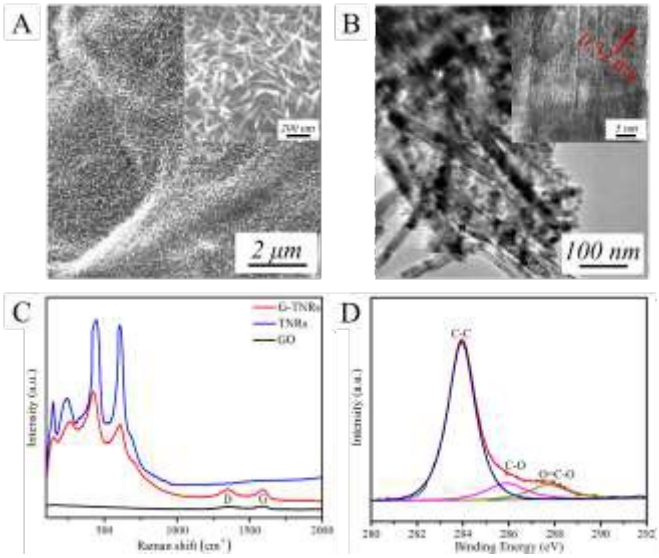

Fig.2 SEM (A), TEM (B) and HRTEM (inset of B) images of G-TNRs. (C) Raman images of G-TNRs, TNRs, GO, respectively. (D) High-resolution XPS spectra of C1s for G-TNRs.

electrocatalysis, photocatalysis and photoelectrocatalysis, but also provides new energy technology of realizing synergistic energy conversion of chemical energy and solar energy.

Fig. 1 shows the working principle of the proposed PEC fuel cell. Upon illumination, electrons were excited from valence band (VB) to conduction band (CB) of TiO_2, while photogenerated holes were generated at the VB of TiO_2. Different from the traditional electrocatalytic oxidation mechanism, methanol was used here as electron donors and successfully oxidized by the photogenerated holes (Detailed reaction mechanism has been described in the ESI). Photogenerated electrons were transported quickly by graphene and flowed to the cathode through an external circuit, where the oxygen was efficiently reduced.

The morphology of GO, TiO_2 nanorods (TNRs), and G-TNRs was characterized by SEM and TEM. As seen in Fig. S1A, the surface of graphene oxide (GO) sheets was smooth and clean. For comparison, after hydrothermal process, evenly distributed and upstanding modified nanorods were clearly observed on the surface of RGO sheets (Fig. 2A), indicating the successful combination of TiO_2 with RGO. In addition, all of the TiO_2 nanorods observed on the surface of RGO sheets exhibited uniform sizes in length (ca. 250 nm) and diameter (ca. 40 nm), as displayed in the inset of Fig. 2A. For comparison, pure TNRs were also prepared and collected on ITOs following the same preparation procedures, as shown in Fig. S1B. Since the TNRs were grown on a flat ITO substrate, these rods were vertically upward. Fig. 2B shows the TEM image of G-TNRs, revealing clearly the morphology characteristics of nanorods. Inset of Fig. 2B shows the well-crystallized structure with fringe spacing of 0.32 nm corresponding well to that of the lattice space of (110) of rutile TiO_2, which is consistent with the highly symmetric selected area electron diffraction pattern (Fig. S2).

The crystalline structure of the synthesized composites was analysed by X-ray diffraction (XRD) and shown in (Fig. S3A). The strong XRD diffraction peak at 27.4º indicated that the TiO_2 nanorods were highly crystallized with a primary rutile phase. Moreover, the XRD diffraction peak at 10.5º of GO disappeared for the G-TNRs sample, indicating that the GO has been successfully reduced after calcinations. [24] Furthermore, Raman spectra of GO, G-TNRs and TNRs were displayed in Fig. 2C. Generally, D (near 1300 cm^{-1}) and G (near 1500 cm^{-1}) peaks were typical characteristic peaks of carbon crystal. The ratio of the intensity of D peak to that of G peak (ID/IG) indicates the degree of disorder from graphite structure. It is obvious that G-TNTs had increased ID/IG of 0.98, compared to that of GO 0.79. In other words, GO was simultaneously reduced during the preparation of rutile TiO_2 nanorods. For G-TNRs and TNRs, the peaks of 130, 255, 490, and 610 cm^{-1} should be attributed to rutile TiO_2. [29] It was found that the intensity of these peaks for the G-TNRs composite slightly decreased in comparing to TNRs, which should be possibly attributed to the interaction between TiO_2 and graphene.

The high resolution of C 1s XPS spectra of G-TNRs were shown in Fig. 2D. Three types of carbon bonds at 284.5 eV, 286.7 eV and 288.5 eV of GO (Fig. S3B) were corresponding to C-C, C-O, C=O-O, respectively. Due to the loss of oxygen-containing functional groups in G-TNRs, the intensity of the peak at 286.7 eV and 288.5 eV tended to be lower. Especially, the intensity of the peak for C-O in G-TNRs was sharply reduced, indicating the successful reduction of GO and the combination of TiO_2 with RGO. [24, 30] We noted that this observation is in accordance with the FTIR spectra (Fig. S3C). For the GO, a mass of oxygenated groups, such as C-O (1069 cm^{-1}), C-O-C (1384 cm^{-1}) and C=O (1730 cm^{-1}) [31, 32] were observed. However, for G-TNRs, some oxygenated groups almost vanished and the peak intensities of the remained oxygenated groups were apparently decreased. The absorption peak at 719 cm^{-1} can be assigned to Ti-O-Ti of TiO_2. As seen, the Ti-O-Ti of G-TNRs was shifted to a lower wavelength of 663 cm^{-1}. According to the previous reported work, this shift was caused by the interaction between graphene and TNRs. [24]

The UV-vis absorption spectra for pure TNRs and G-TNRs composites were shown in Fig. 3A. It can be seen, pure TNRs showed a 3.0 eV (410 nm) rutile-phase band-edge absorption, which was consistent with the TEM and XRD results. After the introduction of graphene, G-TNRs composites showed a slightly red-shift in the absorption edge. Furthermore,

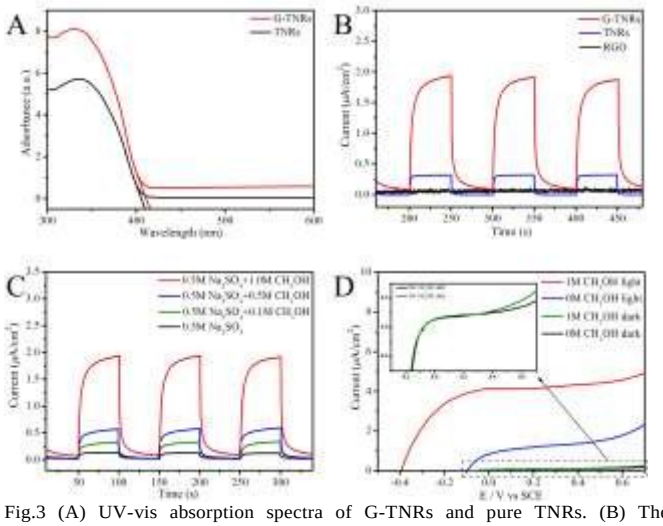

Fig.3 (A) UV-vis absorption spectra of G-TNRs and pure TNRs. (B) The photocurrent responses of GO, pure TNRs and G-TNRs in the presence of 1 M methanol to a light excitation at 360 nm. (C) The photocurrent responses of G-TNRs in the presence of 0, 0.1, 0.5, and 1 M methanol to a light excitation at 360 nm. (D) LSVs of G-TNRs composites measured in a 0.5 M Na_2SO_4 solution electrolyte with or without methanol in the dark and under visible light irradiation.

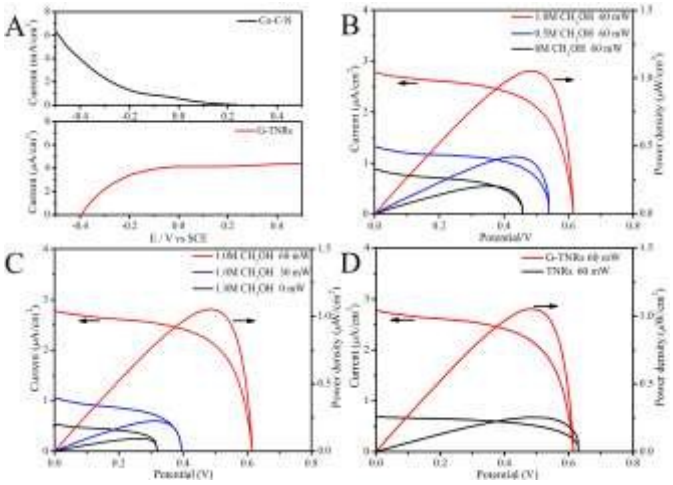

Fig.4 (A) LSV of G-TNRs in 0.5 M Na_2SO_4 solution containing 1.0 M methanol and LSV of GN-CNT in O_2 saturated 0.5 M Na_2SO_4 solution. (B) V-I and P-I operating with light irradiation (solar simulator) of 60 mW·cm^{-2} in 0.5 M Na_2SO_4 solution containing 0 M, 0.5 M and 1.0 M methanol. (C) V-I and P-I curves of the cell operating with 1 M methanol in 0.5 M Na_2SO_4 solution, under light irradiation (solar simulator) of 0 mWcm^{-2}, 30 mW·cm^{-2} and 60 mW·cm^{-2}. (D) V-I and P-I curves of the cell obtained with 1M methanol in 0.5 M Na_2SO_4 solution under light irradiation (solar simulator) of 60 mW·cm^{-2}, the photoanode is TNRs and G-TNRs, respectively.

the light-absorption of G-TNRs was significantly enhanced in ultraviolet region and also slightly improved in visible region, which should be ascribed to the introduction of graphene. To investigate the relationship of light wavelength with the produced photocurrent, the photocurrent was recorded under different wave length at a bias of 0.2 V, as shown in Fig. S4A. It was found that the photocurrent of G-TNRs electrode showed significantly enhancement at the whole irradiation wave length (280-420). Both G-TNRs and TNRs showed a maximum absorption at 360 nm. This was slightly different with the result of the UV-vis absorption spectra. This observation should be explained by the fact that the test was conducted in solution, while UV-vis test was performed using solid powder sample. In order to verify the improvement of the PEC properties of G-TNRs, amperometric i-t curves were recorded in 0.5 M Na_2SO_4 with 1.0 M methanol under 360 nm light irradiation (input power 0.5 mW), as shown in Fig. 3B. For each switch on / off event, both TNRs and G-TNRs electrodes showed a fast and uniform photocurrent response. Remarkably, under irradiation, the photocurrent of G-TNRs electrode was approximately 7 times higher than that of pure TNRs electrode, and nearly no light response was recorded for graphene electrode. The results strongly demonstrate that the PEC performance of G-TNRs was improved significantly after the introduction of graphene. To clearly confirm the PEC oxidation of methanol at the G-TNRs electrode, photocurrents were recorded at different methanol concentration, as shown in Fig. 3C. Upon UV irradiation (360 nm), the photocurrent showed a linear increase with the increase of methanol concentration.

In order to investigate the PEC performance of G-TNRs under the sunlight, LSVs of a G-TNRs electrode were studied under illumination of solar simulator or in darkness. Fig. 3D showed that oxidation current of the G-TNRs electrode under illumination with 100 mW·cm^{-2} of sunlight was much higher than that observed in the darkness. The photocurrent density could reach 2.2 μA·cm^{-2} at a bias of 0.7 V vs. SCE in 0.5 M Na_2SO_4, and the onset oxidation potential for H_2O was -0.1 V. However, after the addition of 1.0 M methanol, the photo-current density could be increased to 4.9 μA·cm^{-2} and the onset oxidation potential was negatively shifted to -0.4 V. Methanol could act as better sacrificial electron donor than water and the photogenerated electron-hole could be separated quickly, which resulted in the enhancement of PEC responses and the decrease of the overpotential.[2] For practical applications, stability of the photocatalyst also should be considered. Fig. S4B presents the durability test of G-TNRs and TNRs under continuous light irradiation. As seen, both G-TNRs and TNRs exhibited high stability even after 10,000 s measurement.

In order to validate the feasibility of the proposed PEC methanol fuel cell, we examined the electrochemical properties of the GN-CNT electrode by LSVs in O_2 saturated 0.5 M Na_2SO_4 solution. GN-CNT was prepared according to our previous work and used as cathode material. As shown in Fig. 4A, the ORR current of GN-CNT electrode could reach 6.3 mA·cm^{-2}, indicating the superior ORR properties of the GN-CNT electrode. The morphological feature of the GN-CNT was characterized by SEM, as shown in Fig. S5. The onset reduction potential for ORR was 0.22 V, which was much higher than the onset oxidation potential observed at G-TNRs electrode. Thereby, the observed results strongly demonstrated that the fabrication of a PEC methanol fuel cell was thermodynamically available. The schematic diagram of photoelectrochemical methanol fuel cell was depicted in Fig. 1 and the cell was fabricated by coupling G-TNRs as photoanode with a GN-CNT modified electrode as cathode. Fig. 4B shows the cell polarization curves (V-I) and cell power output curves (P-I) operating under sunlight irradiation of 60 mW·cm^{-2} in 0.5 M Na_2SO_4 solution containing different amount of methanol. It can be obviously observed that the open circuit voltage and power density increased with the increase of methanol concentration, which was in agreement with the results of Fig.

3C. We noted that, in this PEC fuel cell configuration, methanol served as a representative organic fuel, which was effectively photocatalytical oxidized at the photoanode. In addition, the effect of the irradiation power was explored, as shown in Fig. 4C. The open circuit voltage and power density with sunlight irradiation of 60 $mW \cdot cm^{-2}$ in 0.5 M Na_2SO_4 solution containing 1.0 M methanol showed a significantly increase than that in dark, and the increase of open circuit voltage and power density was directly proportional to the power of irradiation. It indicates that G-TNRs was an efficient photocatalyst that not only photocatalytically oxidized the methanol fuel, but also partially converted the solar energy into electricity. Also, it is reasonable to conclude that the performance of the fuel cell can be improved either by utilizing higher power of light irradiation, or by using higher concentration of methanol. For a control experiment, we examined the performance of PEC methanol fuel cell based on TNRs photoanode, as shown in Fig. 4D. Compared to G-TNRs based fuel cell, the open circuit voltage of TNRs based fuel cell showed no significant difference. However, the power density of the cell based on G-TNRs photoanode was nearly 5 times higher than that of the cell based on TNRs photoanode. It suggests that the performance of a PEC methanol fuel cell could be significantly improved by using rationally designed G-TNRs as photoanode.

In summary, we have demonstrated the synthesis of aligned TiO_2 nanorods decorated graphene composites as a novel photocatalyst. 1D TiO_2 nanorods were uniformly upright grown on 2D graphene nanosheet offered a unique structure that beneficial to facilitate the electron transport and increase the contacted area with the electrolyte and light. Photocatalytic activity of G-TNRs was remarkably enhanced in comparing with TNRs. Importantly, we have proposed a conceptual PEC methanol fuel cell by utilizing G-TNRs as a high performance phtoanode. It should be noted that the power density of this fuel cell still need to be improved for practical application. Future direction of the research should not only include the development of more efficient photocatalysts, but also focus on building more effective fuel cells models based on rationally choose the photoanode and cathode. Nevertheless, this work opens new opportunity for synthesis of 3D nanostructured photocatalyst and raises a novel avenue for synergistic energy recovery from chemical energy and solar energy.

Financial support from National Natural Science Foundation of China (grant no. 21175012, 21575016), and the Chinese Ministry of Education (Project of New Century Excellent Talents in University) is gratefully acknowledged.

Notes and references

1. Y. Yan, J. Fang, Z. Yang, J. Qiao, Z. Wang, Q. Yu and K. Sun, Chemical Communications, 2013, 49, 8632-8634.
2. L. Han, S. Guo, M. Xu and S. Dong, Chemical Communications, 2014, 50, 13331-13333.
3. Y. Du, Y. Feng, Y. Qu, J. Liu, N. Ren and H. Liu, Environmental science & technology, 2014, 48, 7634-7641.
4. L. Zhang, Z. Xu, B. Lou, L. Han, X. Zhang and S. Dong, ChemSusChem, 2014, 7, 2427-2431.
5. R. Chong, Z. Wang, J. Li, H. Han, J. Shi and C. Li, RSC Advances, 2014, 4, 47383-47388.
6. Z. Zhang and H. Wu, RSC Advances, 2014, 4, 37395-37399.
7. L. Zhang, L. Bai, M. Xu, L. Han and S. Dong, Nano Energy, 2015, 11, 48-55.
8. L. Zhang, W. Wang, S. Sun and D. Jiang, Applied Catalysis B: Environmental, 2015, 168, 9-13.
9. S. Guo, D. Li, Y. Zhang, Y. Zhang and X. Zhou, Electrochimica Acta, 2014, 121, 352-360.
10. C. Luo, D. Li, W. Wu, C. Yu, W. Li and C. Pan, Applied Catalysis B: Environmental, 2015, 166, 217-223.
11. F. Kayaci, S. Vempati, C. Ozgit-Akgun, I. Donmez, N. Biyikli and T. Uyar, Nanoscale, 2014, 6, 5735-5745.
12. S. Hernández, V. Cauda, A. Chiodoni, S. Dallorto, A. Sacco, D. Hidalgo, E. Celasco and C. F. Pirri, ACS applied materials & interfaces, 2014, 6, 12153-12167.
13. T. Huo, X. Zhang, X. Dong, X. Zhang, C. Ma, G. Wang, H. Ma and M. Xue, Journal of Materials Chemistry A, 2014, 2, 17366-17370.
14. I. Bretos, R. Jiménez, D. Pérez‐Mezcua, N. Salazar, J. Ricote and M. L. Calzada, Advanced Materials, 2015, 27, 2608-2613.
15. D. Ding, K. Liu, S. He, C. Gao and Y. Yin, Nano letters, 2014, 14, 6731-6736.
16. L. Jing, H. L. Tan, R. Amal, Y. H. Ng and K.-N. Sun, Journal of Materials Chemistry A, 2015, 3, 15675-15682.
17. L. Jing, M. Wang, X. Li, R. Xiao, Y. Zhao, Y. Zhang, Y.-M. Yan, Q. Wu and K. Sun, Applied Catalysis B: Environmental, 2015, 166, 270-276.
18. M. J.-C. Nalbandian, K. E. Greenstein, D. Shuai, M. Zhang, Y.-h. Choa, G. F. Parkin, N. V. Myung and D. M. Cwiertny, Environmental science & technology, 2015.
19. J. Zhang, Y. Wu, M. Xing, S. A. K. Leghari and S. Sajjad, Energy & Environmental Science, 2010, 3, 715-726.
20. S.-m. Chang and W.-s. Liu, Applied Catalysis B: Environmental, 2014, 156, 466-475.
21. S. H. Hwang, J. Yun and J. Jang, Advanced Functional Materials, 2014, 24, 7619-7626.
22. N. Mojumder, S. Sarker, S. A. Abbas, Z. Tian and V. Subramanian, ACS applied materials & interfaces, 2014, 6, 5585-5594.
23. S. Sadhu and P. Poddar, Journal of Physical Chemistry C, 2014, 118, 19363-19373.
24. X. Cao, G. Tian, Y. Chen, J. Zhou, W. Zhou, C. Tian and H. Fu, Journal of Materials Chemistry A, 2014, 2, 4366-4374.
25. W. Fan, Q. Lai, Q. Zhang and Y. Wang, The Journal of Physical Chemistry C, 2011, 115, 10694-10701.
26. S. Yang, C. Cao, P. Huang, L. Peng, Y. Sun, F. Wei and W. Song, Journal of Materials Chemistry A, 2015, 3, 8701-8705.
27. C. Chen, W. Cai, M. Long, B. Zhou, Y. Wu, D. Wu and Y. Feng, Acs Nano, 2010, 4, 6425-6432.
28. Z.-Y. Yang, Y.-F. Zhao, Q.-Q. Xiao, Y.-X. Zhang, L. Jing, Y.-M. Yan and K.-N. Sun, ACS applied materials & interfaces, 2014, 6, 8497-8504.
29. L. He, R. Ma, N. Du, J. Ren, T. Wong, Y. Li and S. T. Lee, Journal of Materials Chemistry, 2012, 22, 19061-19066.
30. N. Yang, Y. Liu, H. Wen, Z. Tang, H. Zhao, Y. Li and D. Wang, ACS nano, 2013, 7, 1504-1512.
31. G. Hu and B. Tang, Materials Chemistry and Physics, 2013, 138, 608-614.
32. P. K. Dubey, P. Tripathi, R. Tiwari, A. Sinha and O. Srivastava, International Journal of Hydrogen Energy, 2014, 39, 16282-16292.